# Origin of anisotropic nonmetallic transport in the $Al_{80}Cr_{15}Fe_5$ decagonal approximant

J. Dolinšek, P. Jeglič, M. Komelj, and S. Vrtnik
*J. Stefan Institute, University of Ljubljana, Jamova 39, SI-1000 Ljubljana, Slovenia*

Ana Smontara, I. Smiljanić, A. Bilušić,* J. Ivkov, and D. Stanić
*Institute of Physics, Bijenička 46, P.O. Box 304, HR-10001 Zagreb, Croatia*

E. S. Zijlstra
*Theoretische Physik, Universität Kassel, D-34132 Kassel, Germany*

Birgitta Bauer and P. Gille
*Institut für Kristallographie und Angewandte Mineralogie, Ludwig-Maximilians-Universität München, Theresienstrasse 41, D-80333 München, Germany*

(Received 11 June 2007; revised manuscript received 13 September 2007; published 20 November 2007)

We present a study of the anisotropic transport properties (electrical resistivity, thermoelectric power, Hall coefficient, and thermal conductivity) of a single-crystalline $Al_{80}Cr_{15}Fe_5$ complex metallic alloy that is an excellent approximant to the decagonal quasicrystal with six atomic layers in one periodic unit. Temperature-dependent electrical resistivity along the *b* and *c* crystalline directions shows a nonmetallic behavior with a broad maximum, whereas it shows a metallic positive temperature coefficient along the *a* direction perpendicular to the (*b*,*c*) atomic planes. *Ab initio* calculations of the electronic density of states reveal that the nonmetallic transport occurs in the presence of a high density of charge carriers. The very different temperature-dependent electrical resistivities along the three crystalline directions can all be treated within the same physical model of slow charge carriers due to weak dispersion of the electronic bands, where the increased electron-phonon scattering upon raising the temperature induces transition from dominant Boltzmann (metallic) to dominant non-Boltzmann (insulatinglike) regime. The temperature dependence of the resistivity is governed predominantly by the temperature dependence of the electronic diffusion constant *D* and the transition has no resemblance to the Anderson-type metal-to-insulator transition based on the gradual electron localization. Structural considerations of the $Al_{80}Cr_{15}Fe_5$ phase show that the anisotropy of the transport properties is a consequence of anisotropic atomic order on the scale of nearest-neighbor atoms, suggesting that the role of quasiperiodicity in the anisotropic transport of decagonal quasicrystals is marginal. We also present a relaxed version of the $Al_4(Cr,Fe)$ structural model by Deng *et al.* [J. Phys.: Condens. Matter **16**, 2283 (2004)].

DOI: 10.1103/PhysRevB.76.174207 PACS number(s): 61.44.Br, 71.23.Ft

## I. INTRODUCTION

One of the basic open questions in the physics of quasicrystals (QCs) is whether quasiperiodicity of the structure influences the physical properties of a solid in a fundamental way by introducing qualitatively new phenomena or the unusual properties are rather a consequence of complex local atomic order with no direct relationship to the quasiperiodicity. Being metallic alloys, the most striking property of QCs is their nonmetallic electrical resistivity with negative temperature coefficient (NTC) along the quasiperiodic direction. Decagonal (*d*) phases are of special importance, as their structure can be viewed as a periodic stack of quasiperiodic planes, so that *d*-QCs are two-dimensional QCs, whereas they are periodic crystals in a direction perpendicular to the quasiperiodic planes. The resistivity in the quasiperiodic (*Q*) and periodic (*P*) directions can be consequently investigated on the same sample. Literature reports reveal that *d*-QCs exhibit anisotropy in their electronic and thermal transport properties [electrical resistivity $\rho$,[1–3] thermoelectric power *S*,[4] Hall coefficient $R_H$,[5,6] thermal conductivity $\kappa$,[7,8] and optical conductivity $\sigma(\omega)$ (Ref. 9)], when measured along the *Q* and *P* directions. The degree of anisotropy is related to the structural details of a particular decagonal phase, depending on the number of quasiperiodic layers in one periodic unit.[10,11] The most anisotropic cases are the phases with just two layers, realized in *d*-Al-Cu-Co and *d*-Al-Ni-Co, where the periodicity length along the periodic axis is about 0.4 nm and the resistivity ratio at room temperature (RT) amounts typically $\rho_Q/\rho_P \approx 6-10$.[1–3] Other *d* phases contain more quasiperiodic layers in a periodic unit and show smaller anisotropies. In *d*-Al-Co, *d*-Al-Ni, and *d*-Al-Si-Cu-Co, there are four quasiperiodic layers with periodicity about 0.8 nm and the RT anisotropy is $\rho_Q/\rho_P \approx 2-4$.[4] *d*-Al-Mn, *d*-Al-Cr, and *d*-Al-Pd-Mn phases contain six layers with periodicity of about 1.2 nm and the anisotropy amounts $\rho_Q/\rho_P \approx 1.2-1.4$, whereas *d*-Al-Pd and *d*-Al-Cu-Fe phases with eight layers in a periodicity length of 1.6 nm are close to isotropic. A common property of *d* phases is their metallic resistivity in the periodic direction, $\rho_P$, showing positive temperature coefficient (PTC) at metallic values (e.g., $\rho_P^{300\ \mathrm{K}} \approx 40\ \mu\Omega$ cm in *d*-Al-Cu-Co and *d*-Al-Ni-Co),[2] whereas the considerably larger resistivity $\rho_Q$ in the quasiperiodic plane (e.g., $\rho_Q^{300\ \mathrm{K}} \approx 330\ \mu\Omega$ cm)[2] exhibits a NTC and usually also a maximum somewhere below RT or a leveling off upon $T \to 0$. At

 

present, there is no unified theory to explain the very different temperature dependencies of $\rho_P$ and $\rho_Q$ within the same physical picture. While $\rho_P$ was considered to be consistent with the semiclassical Bloch-Grüneisen theory of electron-phonon scattering in regular metals,[2,11] nonmetallic $\rho_Q$ was proposed to be described by the generalized Faber-Ziman theory that considers enhanced electron-phonon interaction and enhanced phonon-phonon coupling in the quasiperiodic plane.[3] The NTC and the maximum in $\rho_Q$ were consequently attributed to the temperature-dependent Debye-Waller factor $e^{-2W} \approx 1 - \beta T$. In another approach, $\rho_Q$ was attributed to phonon-assisted tunneling of electrons in the regime of extended states.[2,11] The existence of a pseudogap in the electronic density of states (DOS) at the Fermi energy $E_F$ and its role in the electronic transport of *d*-QCs are another pending issue. Photoemission experiments[12] have demonstrated that the pseudogap at $E_F$, characteristic of many icosahedral QCs, is absent in *d* alloys, in agreement with more recent theoretical studies.[13] Experiments and DOS calculations on *d*-Al-Ni-Co and *d*-Al-Cu-Co decagonal approximants also suggest that the DOS value at $E_F$ is high.[14] The nonmetallic electrical transport in the presence of a high number of electrical carriers is thus another open issue in the context of *d*-QCs. Moreover, anisotropies in the electronic and thermal transport properties similar to those in *d*-QCs were also observed in periodic structurally complex phases $Al_{13}Co(Fe)_4$ and the Taylor-phase $Al_3Mn$,[15] so that quasiperiodicity alone cannot be the origin of the anisotropic transport. We are thus left with the following open questions: (i) What is the origin of nonmetallic transport in the presence of a high density of charge carriers? (ii) Does there exist a unified picture of the electronic transport along the *Q* and *P* directions in *d*-QCs, i.e., can the very different magnitudes and temperature dependencies of $\rho_Q$ and $\rho_P$ be explained within the same physical model? (iii) What is the role of quasiperiodicity (is there any) in the anisotropic transport of *d*-QCs? We address these fundamental questions by presenting an experimental and theoretical study of transport properties (electrical resistivity, thermopower, Hall coefficient, and thermal conductivity) along the three crystalline directions of a single-crystalline $Al_4(Cr,Fe)$ complex metallic alloy that is an excellent approximant to the decagonal phase with six atomic layers in a periodic unit.

## II. SAMPLE PREPARATION

The investigated $Al_4(Cr,Fe)$ compound belongs to the class of body-centered orthorhombic phases $Al_4TM$ (transition metal) with $a \approx 1.25$ nm, $b \approx 1.25$ nm, and $c \approx 3.05$ nm, which coexist with the *d*-QC having a period of 1.25 nm along its periodic tenfold direction (corresponding to the *a* axis of $Al_4TM$).[16] The $Al_4TM$ phase has been so far observed in no less than six different Al-TM alloys, so that it must be a common structure to this class of alloys. The $Al_4TM$ structure can be described as a periodic repetition of a sequence $P'FPp'fp$ of six atomic layers stacked within one periodicity length of 1.25 nm along *a*, showing close structural relationship to the six-layer Al-TM *d*-QCs with the same periodicity. The block $P'FP$ is composed of a flat layer *F* at $x=0$ and a puckered layer *P* at $x \approx a/6$, whereas the puckered layer $P'$ is in mirror-reflecting position across the *F* layer. The block $p'fp$ equals the block $P'FP$ translated by $(a/2, b/2, c/2)$.

The single crystal used in our study was grown from an incongruent Al-rich melt of initial composition $Al_{87}Cr_7Fe_6$ by the Czochralski method using a native seed. The composition of the sample (rounded to the closest integers) was $Al_{80}Cr_{15}Fe_5$ and its structure could be assigned to the orthorhombic phase, previously described by Deng *et al.*,[16] with the following crystallographic parameters: Pearson's symbol *oI*366-59.56, space group *Immm* (No. 71), unit cell parameters $a=1.2500(6)$ nm, $b=1.2617(2)$ nm, and $c=3.0651(8)$ nm, and 306.44 atoms in the giant unit cell. Due to body centering, the primitive unit cell contains only half as many atoms. Cr and Fe atoms are not differentiated crystallographically. In order to perform crystalline-direction-dependent studies, we prepared three bar-shaped samples of dimensions $2 \times 2 \times 8$ mm$^3$ with their long axes along the three crystallographic directions of the orthorhombic unit cell. The [100] direction (designated in the following as *a*) corresponds to the periodic direction in *d*-QCs, whereas the [010] (*b*) and [001] (*c*) directions lie within the atomic planes (corresponding to the quasiperiodic directions in *d*-QCs).

## III. TRANSPORT PROPERTIES

### A. Electrical resistivity

Electrical resistivity was measured between 300 and 2 K using the standard four-terminal technique and the data are displayed in Fig. 1. The resistivity is the lowest along the *a* axis perpendicular to the atomic planes. $\rho_a$ shows a PTC in the whole investigated temperature interval and a RT value $\rho_a^{300\ \mathrm{K}}=297\ \mu\Omega$ cm. The resistivities within the atomic planes are higher and exhibit different temperature dependencies with a broad maximum, where the temperature coefficient is reversed. $\rho_b$ exhibits a maximum at about 125 K with the peak value 375 $\mu\Omega$ cm and the RT value $\rho_b^{300\ \mathrm{K}}=371\ \mu\Omega$ cm. The resistivity $\rho_c$ is the highest; its maximum value 413 $\mu\Omega$ cm occurs at 100 K and the RT value is $\rho_c^{300\ \mathrm{K}}=407\ \mu\Omega$ cm. At RT, the ratios of the resistivities are $\rho_c/\rho_a=1.37$, $\rho_b/\rho_a=1.25$, and $\rho_c/\rho_b=1.10$. The resistivity of $Al_{80}Cr_{15}Fe_5$ is thus analogous to *d*-QCs,[2–4] where the resistivity perpendicular to the quasiperiodic atomic planes also shows a metallic PTC and its value is smaller than the in-plane resistivity, which exhibits a nonmetallic character with NTC on the high-temperature side of the maximum in $\rho$ and PTC below.

### B. Thermoelectric power

The thermoelectric power (the Seebeck coefficient *S*) was measured between 300 and 4 K by applying a differential method with two identical thermocouples (Chromel gold with 0.07% iron), attached to the sample with silver paint, and the data are displayed in Fig. 2. Thermopower is small in all three directions and the values are in the range between +1 and −2.5 $\mu$V/K. $S_a$, $S_b$, and $S_c$ exhibit slight quantitative

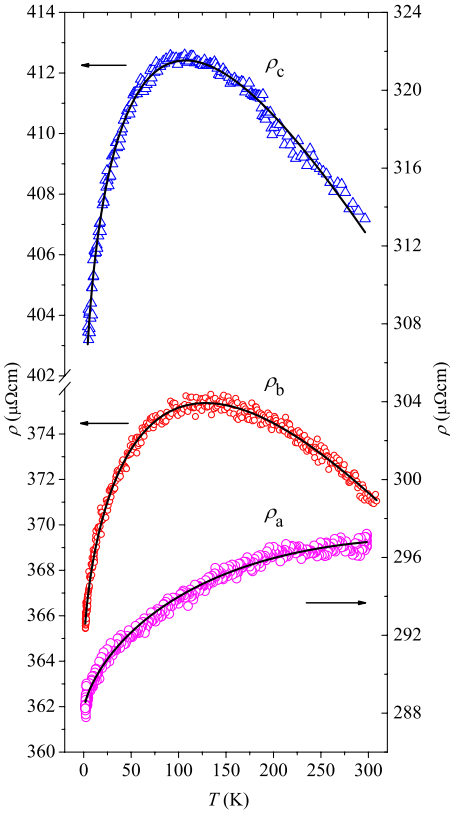


FIG. 1. (Color online) Temperature-dependent electrical resistivity of $Al_{80}Cr_{15}Fe_5$ along the three crystalline directions $a$, $b$, and $c$ of the orthorhombic unit cell. Solid lines are fits with Eq. (2) and the fit parameter values are given in Table III.

differences in the details of their rather complicated temperature dependencies, but all of them exhibit qualitatively similar features of a pronounced minimum around 80 K and additional local minima and maxima. In the minimum at 80 K, $S_a$ value is the smallest, whereas at elevated temperatures, $S_a$ exhibits stronger growth than the in-plane coefficients $S_b$ and $S_c$.

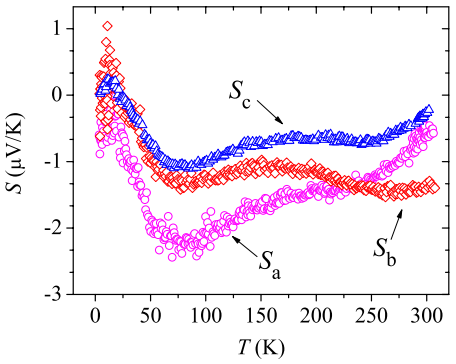


FIG. 2. (Color online) Thermoelectric power of $Al_{80}Cr_{15}Fe_5$ along the three crystalline directions $a$, $b$, and $c$ of the orthorhombic unit cell.

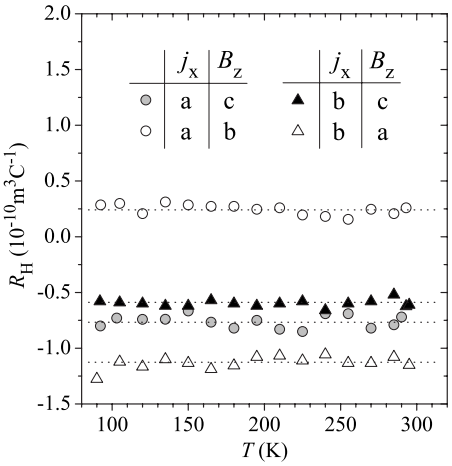


FIG. 3. Temperature-dependent Hall coefficient of $Al_{80}Cr_{15}Fe_5$ for different combinations of directions of the current $j_x$ and the magnetic field $B_z$ (given in the legend).

### C. Hall coefficient

The Hall effect measurements were performed by the five-point method using standard ac technique in magnetic fields up to 1 T. The current through the samples was in the range 10–50 mA and its actual value was selected with the requirement that the self-heating of the sample did not increase its temperature above the sample-holder temperature for more than 1 K. The temperature-dependent Hall coefficient $R_H = E_y / j_x B_z$ is displayed in Fig. 3. In the first set of experiments, the current $j_x$ was directed along the $a$ direction perpendicular to the atomic planes and the magnetic field $B_z$ was applied along either of the two in-plane crystalline directions ($b$ and $c$). In the second set, the current was flowing in plane along $b$, whereas the field pointed either along the second in-plane direction $c$ or perpendicular to the planes along $a$. The results are collected in Table I. In all cases, $R_H$ shows a metallic behavior by being temperature independent (within the experimental uncertainty of $\pm 0.1 \times 10^{-10}$ m$^3$ C$^{-1}$) at typical metallic values in the range about $\pm 1 \times 10^{-10}$ m$^3$ C$^{-1}$. $R_H$ exhibits pronounced anisotropy. While $R_H = E_c / j_a B_b$ is positive, the other three combinations of directions yield negative Hall coefficients.

### D. Electronic density of states

In the electronic transport phenomena, an important quantity is the electronic DOS at the Fermi level. We performed

TABLE I. Anisotropic Hall coefficient in $Al_{80}Cr_{15}Fe_5$ for various directions of the current and field.

| Current direction ($j_x$) | Field direction ($B_z$) | $R_H$ ($10^{-10}$ m$^3$ C$^{-1}$) |
|---|---|---|
| $a$ | $b$ | +0.23 |
| | $c$ | −0.76 |
| $b$ | $a$ | −1.12 |
| | $c$ | −0.60 |

an *ab initio* electronic structure study of $Al_4(Cr,Fe)$ with the full-potential linearized augmented plane wave (LAPW) computer program WIEN2K,[17] which is based on the density functional theory. For our calculations, we used the local density approximation of Perdew and Wang.[18] Important details of the calculations are as follows. The radii of the muffin-tin spheres around the atoms were 2.06 Å for the Al atoms, 2.11 Å for the Cr atoms, and 2.35 Å for the Fe atoms. The Cr $3p$ and Fe $3p$ semicore states, which are not well localized within the muffin-tin spheres (more than 0.01 $e$/atom "leak" out of the spheres), were treated as full valence states using local orbitals.[19] This treatment ensured the orthogonality of the higher-lying valence states with the semicore states. Apart from the local orbitals for the semicore states, the basis further included LAPWs with energies up to 127 eV and additional local orbitals for the Al $3d$, Cr $3d$, and Fe $3d$ states using the formalism described elsewhere.[20,21] The **k** space was sampled with 16 special **k** points (corresponding to 64 **k** points in the entire Brillouin zone) using temperature smearing (the electronic temperature was $T_e$=2 mRy).

In the $Al_4(Cr,Fe)$ model of Deng *et al.*,[16] no distinction is made between the Cr and Fe sites. In addition, there exist sites of mixed and partial occupancies. For our calculations, where each site must be either vacant or occupied by a specific atom, we made the following choices: (1) the sites of mixed occupancy 75% Al and 25% (Cr,Fe) were occupied with Al; (2) to avoid short distances, sites of partial occupancy were occupied in 50% of the cases (though in the structure refinement of the Deng model, the occupancy ranges from 50% to 67%); (3) for the (Cr,Fe) sites, we tried two models, one where neighboring Fe-Fe contacts were avoided as much as possible and another where we tried to avoid Cr-Cr contacts. We found that the first model was more stable, by approximately 2 eV per primitive unit cell, and we used this model as a basis for further *ab initio* calculations. This model had 148 atoms per primitive unit cell (≈153 in the original Deng model) and its composition was $Al_{80.4}Cr_{10.8}Fe_{8.8}$ (compared to $Al_{80.6}Cr_{10.7}Fe_{8.7}$ in the original model).

Calculating the DOS for the model of Deng *et al.*[16] with the sites of mixed and partial occupancies occupied as described above, we found that the forces on some of the atoms were as large as ≈94 mRy/Å. The reason for this is most probably the fact that the model gives atomic positions that are averaged over the different possible occupations of the mixed and partially occupied sites, whereas in our model, we have made specific choices described in the previous paragraph. To bring the atoms to their equilibrium positions, we performed structural relaxation, which was stopped after the forces on all atoms were less than 7 mRy/Å. The final atomic coordinates before and after the structural relaxation are given in Table II. The $y$ and $z$ coordinates of all independent atomic positions are shown in Figs. 4(a) and 4(b), which show the $F$ and $P$ atomic planes, respectively. Figure 4(c) shows the $x$ and $z$ coordinates of all atoms that lie in the plane $y \approx 0$. The first thing to notice in Fig. 4 is that some positions of the original model of Deng *et al.* (indicated by small black dots) are not occupied in our new model. These are the unoccupied half of the above-mentioned partially occupied sites. One can recognize this by realizing that the original model of Deng *et al.* has mirror planes at $x$=0, $y$=0, and $z$=0 and that, due to the particular choices we made for occupying the partially occupied sites, we broke the mirror symmetries across the $y$=0 and $z$=0 planes, but not the mirror symmetry across the $x$=0 plane. As a result, the layered $P'FPp'fp$ structure remained intact. From Figs. 4(a) and 4(b), it is evident that the $y$ and $z$ coordinates of the atoms did not change dramatically upon structural relaxation. This indicates that the model of $Al_4(Cr,Fe)$ of Deng *et al.* is robust against the occupations that we have chosen. The $x$ coordinates in the $F$ plane [Fig. 4(a)] are zero by symmetry and did not change during the structural relaxation. In the original model of Deng *et al.*, the $x$ coordinates in the $P$ plane [shown in Fig. 4(b)] were between 0.1130 and 0.1915 $a$. In the relaxed model, they were between 0.0894 and 0.2271 $a$, so that puckering of the $P$ layer increased somewhat. As a final point, it is remarkable to note how far the two Cr11 atoms in the middle of Fig. 4(c) have moved toward each other: from the original distance of 2.85 Å to 2.24 Å in the relaxed model. We have no immediate explanation for this fact.

The electronic DOSs of the original model of $Al_4(Cr,Fe)$ of Deng *et al.* and our relaxed model are shown in Fig. 5. At about 10 eV below the Fermi energy, the free-electron-like DOS of Al can be clearly recognized. Around 1–2 eV below $E_F$, there is a peak due to the Cr $3d$ and Fe $3d$ states. Comparing the two DOSs, it can be seen that the structural relaxation has caused the DOS at $E_F$ to become somewhat lower, whereas the (Cr,Fe) $3d$ peak has become more pronounced. The lowering of the DOS near $E_F$ indicates further electronic stabilization of the relaxed structure, as compared to the original model with unrelaxed atomic coordinates. For the electronic conduction, it is important to note that the DOS at $E_F$ is high with no tendency to exhibit a pseudogap. The calculated DOS of $Al_4(Cr,Fe)$ is thus metal-like, so that the nonmetallic electrical resistivity displayed in Fig. 1 occurs in the presence of a high density of charge carriers.

### E. Lattice thermal conductivity

The thermal conductivity $\kappa$ of $Al_{80}Cr_{15}Fe_5$ was measured along the three crystallographic directions using an absolute steady-state heat-flow method. The thermal flux through the samples was generated by a 1 kΩ $RuO_2$ chip resistor, glued to one end of the sample, while the other end was attached to a copper heat sink. The temperature gradient across the sample was monitored by a Chromel-Constantan differential thermocouple. The phononic contribution $\kappa_{ph}=\kappa-\kappa_{el}$ was extracted by subtracting the electronic contribution $\kappa_{el}$ from the total conductivity using the Wiedemann-Franz law and the measured electrical resistivity data. Though the use of the Wiedemann-Franz law is a rough approximation, in this way determined $\kappa_{ph}$ gives an indication of the anisotropy of the phononic spectrum. Phononic thermal conductivity is displayed in Fig. 6, where we observe that the conductivity $\kappa_{ph}^a$ along the $a$ direction in the low-$T$ regime below 50 K (which can be associated with the regime where *umklapp* processes are still ineffective) is the highest, whereas the two in-plane

TABLE II. Coordinates of the relaxed model of $Al_4(Cr,Fe)$. The coordinates ($x_D$, $y_D$, $z_D$) of the original model of Deng *et al.* (Ref. 16) are also given for comparison. The labels of the atoms in the first column follow the labeling of Ref. 16, where letters were used to distinguish between split sites.

| Atom | $x$ ($a$) | $y$ ($b$) | $z$ ($c$) | $x_D$ ($a$) | $y_D$ ($b$) | $z_D$ ($c$) |
|---|---|---|---|---|---|---|
| Fe1 | 0 | 0.5013 | 0.5003 | 0 | 0.5 | 0.5 |
| Fe2a | 0 | −0.0083 | 0.1429 | 0 | 0 | 0.1448 |
| Fe2b | 0 | 0.0117 | −0.1420 | 0 | 0 | −0.1448 |
| Cr3a | 0 | 0.1934 | 0.2807 | 0 | 0.1941 | 0.2874 |
| Fe3b | 0 | 0.1900 | −0.2810 | 0 | 0.1941 | −0.2874 |
| Fe3c | 0 | −0.1900 | 0.2800 | 0 | −0.1941 | 0.2874 |
| Cr3d | 0 | −0.1953 | −0.2791 | 0 | −0.1941 | −0.2874 |
| Fe4a | 0 | 0.1218 | 0.4980 | 0 | 0.1057 | 0.5 |
| Cr4b | 0 | −0.1076 | 0.5017 | 0 | −0.1057 | 0.5 |
| Cr5a | 0 | 0.3001 | 0.0694 | 0 | 0.3051 | 0.0733 |
| Fe5b | 0 | 0.3079 | −0.0720 | 0 | 0.3051 | −0.0733 |
| Cr5c | 0 | −0.3070 | 0.0701 | 0 | −0.3051 | 0.0733 |
| Cr5d | 0 | −0.3032 | −0.0696 | 0 | −0.3051 | −0.0733 |
| Fe6a | 0 | 0.3065 | 0.3635 | 0 | 0.2980 | 0.3615 |
| Fe6b | 0 | −0.3015 | −0.3649 | 0 | −0.2980 | −0.3615 |
| Fe7a | 0.3203 | −0.0047 | 0.2304 | 0.3271 | 0 | 0.2363 |
| Fe7b | 0.3203 | 0.0053 | −0.2296 | 0.3271 | 0 | −0.2363 |
| Cr8a | 0 | 0.5005 | 0.2108 | 0 | 0.5 | 0.2134 |
| Cr8b | 0 | 0.4987 | −0.2107 | 0 | 0.5 | −0.2134 |
| Cr9a | 0 | 0.2003 | 0.0027 | 0 | 0.2048 | 0 |
| Cr9b | 0 | −0.2078 | −0.0013 | 0 | −0.2048 | 0 |
| Cr10a | 0.1689 | 0.2014 | 0.0443 | 0.1742 | 0.2018 | 0.0460 |
| Cr10b | 0.1693 | −0.2045 | −0.0452 | 0.1742 | −0.2018 | −0.0460 |
| Cr11 | 0.0894 | 0.0031 | 0.0004 | 0.1139 | 0 | 0 |
| Al1a | 0 | 0.3826 | 0.1459 | 0 | 0.3851 | 0.1473 |
| Al1b | 0 | 0.3878 | −0.1449 | 0 | 0.3851 | −0.1473 |
| Al1c | 0 | −0.3898 | 0.1447 | 0 | −0.3851 | 0.1473 |
| Al1d | 0 | −0.3845 | −0.1461 | 0 | −0.3851 | −0.1473 |
| Al2a | 0 | 0.4001 | 0.2872 | 0 | 0.3963 | 0.2866 |
| Al2b | 0 | 0.3950 | −0.2855 | 0 | 0.3963 | −0.2866 |
| Al2c | 0 | −0.3951 | 0.2856 | 0 | −0.3963 | 0.2866 |
| Al2d | 0 | −0.4003 | −0.2876 | 0 | −0.3963 | −0.2866 |
| Al3a | 0 | −0.0007 | 0.2881 | 0 | 0 | 0.2911 |
| Al3b | 0 | 0.0001 | −0.2885 | 0 | 0 | −0.2911 |
| Al4a | 0 | 0.4978 | 0.0626 | 0 | 0.5 | 0.0652 |
| Al4b | 0 | 0.4980 | −0.0626 | 0 | 0.5 | −0.0652 |
| Al5a | 0 | 0.0954 | 0.0696 | 0 | 0.1010 | 0.0719 |
| Al5b | 0 | 0.1077 | −0.0661 | 0 | 0.1010 | −0.0719 |
| Al5c | 0 | −0.1058 | 0.0659 | 0 | −0.1010 | 0.0719 |
| Al5d | 0 | −0.0975 | −0.0674 | 0 | −0.1010 | −0.0719 |
| Al6a | 0.1914 | 0.4950 | 0.1771 | 0.1915 | 0.5 | 0.1749 |
| Al6b | 0.1926 | 0.5040 | −0.1768 | 0.1915 | 0.5 | −0.1749 |
| Al7a | 0.1793 | 0.3078 | 0.3127 | 0.1911 | 0.3079 | 0.3088 |
| Al7b | 0.1893 | 0.3085 | −0.3085 | 0.1911 | 0.3079 | −0.3088 |
| Al7c | 0.1901 | −0.3103 | 0.3082 | 0.1911 | −0.3079 | 0.3088 |
| Al7d | 0.1799 | −0.3074 | −0.3126 | 0.1911 | −0.3079 | −0.3088 |
| Al8a | 0.1111 | 0.3201 | 0.2232 | 0.1136 | 0.3135 | 0.2207 |

TABLE II. (*Continued.*)

| Atom | $x$ ($a$) | $y$ ($b$) | $z$ ($c$) | $x_D$ ($a$) | $y_D$ ($b$) | $z_D$ ($c$) |
|---|---|---|---|---|---|---|
| Al8b | 0.1119 | 0.3203 | −0.2198 | 0.1136 | 0.3135 | −0.2207 |
| Al8c | 0.1119 | −0.3208 | 0.2201 | 0.1136 | −0.3135 | 0.2207 |
| Al8d | 0.1111 | −0.3208 | −0.2233 | 0.1136 | −0.3135 | −0.2207 |
| Al9a | 0.1865 | 0.0091 | 0.0832 | 0.1850 | 0 | 0.0917 |
| Al9b | 0.1845 | −0.0105 | −0.0829 | 0.1850 | 0 | −0.0917 |
| Al10a | 0.1117 | 0.4930 | 0.3522 | 0.1173 | 0.5 | 0.3507 |
| Al10b | 0.1125 | 0.5072 | −0.3523 | 0.1173 | 0.5 | −0.3507 |
| Al11a | 0.1088 | 0.3702 | −0.0012 | 0.1130 | 0.3844 | 0 |
| Al11b | 0.1115 | −0.3772 | 0.0000 | 0.1130 | −0.3844 | 0 |
| Al12a | 0 | 0.1228 | 0.2035 | 0 | 0.1224 | 0.2095 |
| Al12b | 0 | 0.1277 | −0.2058 | 0 | 0.1224 | −0.2095 |
| Al12c | 0 | −0.1259 | 0.2058 | 0 | −0.1224 | 0.2095 |
| Al12d | 0 | −0.1220 | −0.2028 | 0 | −0.1224 | −0.2095 |
| Al13a | 0 | 0.3108 | 0.4982 | 0 | 0.3011 | 0.5 |
| Al13b | 0 | −0.3060 | 0.5014 | 0 | −0.3011 | 0.5 |
| Al14a | 0.1822 | 0.1201 | 0.2597 | 0.1808 | 0.1198 | 0.2633 |
| Al14b | 0.1807 | 0.1204 | −0.2615 | 0.1808 | 0.1198 | −0.2633 |
| Al14c | 0.1811 | −0.1209 | 0.2616 | 0.1808 | −0.1198 | 0.2633 |
| Al14d | 0.1822 | −0.1199 | −0.2593 | 0.1808 | −0.1198 | −0.2633 |
| Al15a | 0.1789 | 0.0027 | 0.1766 | 0.1788 | 0 | 0.1820 |
| Al15b | 0.1785 | −0.0030 | −0.1763 | 0.1788 | 0 | −0.1820 |
| Al16a | 0.3091 | 0.1124 | 0.4106 | 0.3104 | 0.1127 | 0.4072 |
| Al16b | 0.3091 | 0.1121 | −0.4124 | 0.3104 | 0.1127 | −0.4072 |
| Al16c | 0.3112 | −0.1211 | 0.4138 | 0.3104 | −0.1127 | 0.4072 |
| Al16d | 0.3083 | −0.1175 | −0.4118 | 0.3104 | −0.1127 | −0.4072 |
| Al17a | 0.1120 | 0.1214 | 0.3491 | 0.1199 | 0.1145 | 0.3523 |
| Al17b | 0.1159 | 0.1185 | −0.3523 | 0.1199 | 0.1145 | −0.3523 |
| Al17c | 0.1144 | −0.1274 | 0.3506 | 0.1199 | −0.1145 | 0.3523 |
| Al17d | 0.1122 | −0.1204 | −0.3477 | 0.1199 | −0.1145 | −0.3523 |
| Al18a | 0.3772 | 0.3068 | 0.3712 | 0.3847 | 0.3047 | 0.3639 |
| Al18b | 0.3909 | 0.3063 | −0.3682 | 0.3847 | 0.3047 | −0.3639 |
| Al18c | 0.3909 | −0.3061 | 0.3680 | 0.3847 | −0.3047 | 0.3639 |
| Al18d | 0.3773 | −0.3082 | −0.3707 | 0.3847 | −0.3047 | −0.3639 |
| Al19a | 0.1188 | 0.4039 | 0.4306 | 0.1286 | 0.4013 | 0.4276 |
| Al19b | 0.1178 | −0.4049 | −0.4318 | 0.1286 | −0.4013 | −0.4276 |
| Al20a | 0.2757 | 0.0987 | −0.0147 | 0.3162 | 0.0898 | −0.0213 |
| Al20b | 0.2729 | −0.1002 | 0.0143 | 0.3162 | −0.0898 | 0.0213 |
| Al21 | 0.1731 | 0.0061 | 0.4722 | 0.1869 | 0 | 0.4744 |
| Al22a | 0.1886 | 0.1951 | −0.4849 | 0.1824 | 0.1849 | −0.4796 |
| Al22b | 0.1888 | −0.1963 | 0.4899 | 0.1824 | −0.1849 | 0.4796 |
| Al23a | 0.1135 | 0.1998 | 0.4298 | 0.1161 | 0.1870 | 0.4332 |
| Al23b | 0.1088 | −0.2003 | −0.4276 | 0.1161 | −0.1870 | −0.4332 |
| Al24 | 0.1126 | 0.0111 | −0.4425 | 0.1154 | 0 | −0.4358 |
| Al25a | 0.1870 | 0.3116 | −0.4008 | 0.1835 | 0.3013 | −0.3965 |
| Al25b | 0.1862 | −0.3081 | 0.4009 | 0.1835 | −0.3013 | 0.3965 |
| Al26 | 0 | 0.0106 | 0.4215 | 0 | 0 | 0.4198 |
| Al27a | 0 | 0.1967 | −0.4252 | 0 | 0.1848 | −0.4257 |
| Al27b | 0 | −0.1970 | 0.4261 | 0 | −0.1848 | 0.4257 |

TABLE II. (*Continued.*)

| Atom | $x$ ($a$) | $y$ ($b$) | $z$ ($c$) | $x_D$ ($a$) | $y_D$ ($b$) | $z_D$ ($c$) |
|---|---|---|---|---|---|---|
| Al28a | 0 | 0.4131 | −0.4242 | 0 | 0.4175 | −0.4233 |
| Al28b | 0 | −0.4135 | 0.4246 | 0 | −0.4175 | 0.4233 |

conductivities $\kappa_{ph}^{b}$ and $\kappa_{ph}^{c}$ are somewhat smaller and also show a very weak in-plane anisotropy. The total thermal conductivity $\kappa$ and the electronic contribution $\kappa_{el}$ along the three crystalline directions are displayed in the inset of Fig. 6.

## IV. ANALYSIS

The temperature-dependent electrical resistivity of $Al_{80}Cr_{15}Fe_5$ was analyzed within the theory of Trambly de Laissardière *et al.*,[22] who have shown that the semiclassical (Bloch-Boltzmann) model of conduction breaks down when the mean free path of charge carriers is smaller than a typical extension of their wave function. This situation is realized for sufficiently slow charge carriers and leads to a transition from a metallic to an insulatinglike regime when scattering by defects or temperature effects increases. The semiclassical theory of conduction in crystals is based on the concept of a charge carrier wave packet propagating at a velocity $v_{nj}(\vec{k}) = (1/\hbar)\partial E_n(\vec{k})/\partial k_j$, where $j=x,y,z$ and $E_n(\vec{k})$ is the dispersion relation for band $n$ and wave vector $\vec{k}$. The validity of the wave packet concept requires that the extension $L_{wp}$ of the wave packet of the charge carrier is smaller than the distance $v\tau$ of traveling between two scattering events separated by a time $\tau$ (the so-called ballistic propagation). On the contrary, when $v\tau < L_{wp}$, a condition that can be realized for sufficiently slow charge carriers, the propagation is nonballistic and the semiclassical model breaks down. Small velocities are found in systems with small band dispersion, i.e., when the derivatives $\partial E_n(\vec{k})/\partial k_j$ are small. $d$-QCs are examples of such systems. Electronic band calculations on the Al-Cu-Co decagonal approximant with two atomic layers in one periodicity unit have revealed[11] that the bands are flat (very much dispersionless) in the $Q$ direction, whereas they exhibit more dispersion in the $P$ direction. Consequently, the velocity of charge carriers within the quasiperiodic planes is small, whereas it is larger along the periodic direction.

The theory[22] enables us to treat the standard Boltzmann metallic regime of fast carriers ($v\tau > L_{wp}$) on the same footing with the slow carriers ($v\tau < L_{wp}$) in the insulatinglike regime. According to the Einstein relation, the conductivity

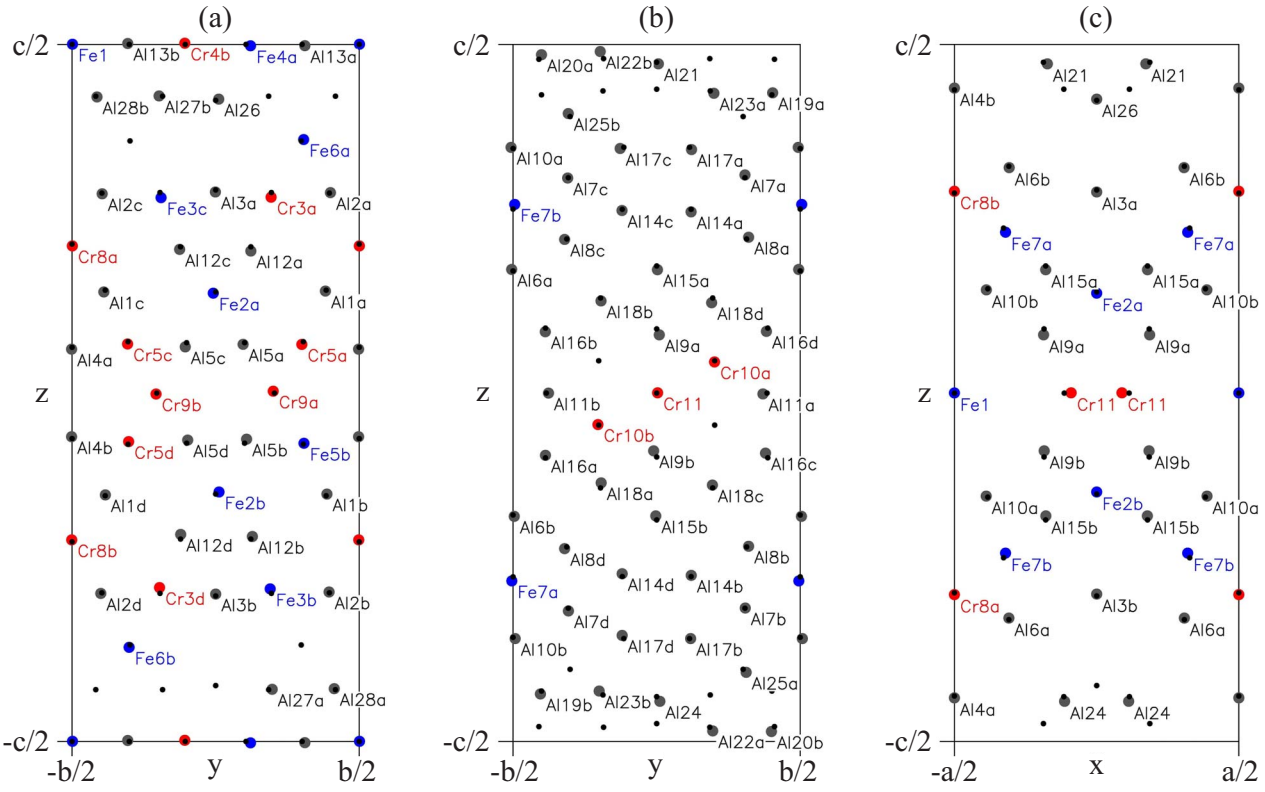


FIG. 4. (Color online) Atomic positions of the relaxed model of $Al_4(Cr,Fe)$, shown by large gray (online colored) circles. The original coordinates published by Deng *et al.* (Ref. 16) are indicated by black dots. The panels show (a) the $x=0$ (flat layer $F$), (b) the $x \approx a/6$ (puckered layer $P$), and (c) the $y=0$ planes.

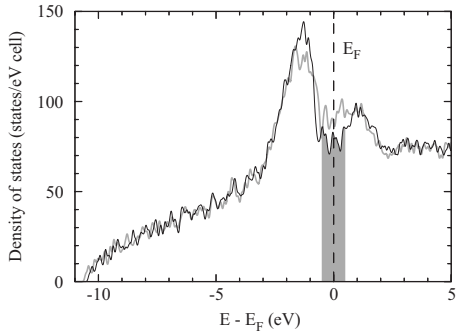


FIG. 5. Theoretical electronic DOSs of the $Al_4(Cr,Fe)$ phase, calculated *ab initio* for the original (unrelaxed) structural model of Deng *et al.* (thick gray curve) and our relaxed model (thin black curve). The gray hatched area around $E_F$ indicates the energy window that was used to calculate the electronic charge density shown in Fig. 8.

$\sigma$ depends on the DOS $g(E)$ and the spectral diffusivity $D(E)$ within the thermal interval of a few $k_BT$ around the Fermi level $E_F$. In cases of slowly varying metallic DOS with no pseudogap at $E_F$, it is permissible to replace $g(E)$ by $g(E_F)$. For the diffusion constant, it was shown[22] that it can be written as $D=v^2\tau+L^2(\tau)/\tau$, where $L^2(\tau)$ is the nonballistic (non-Boltzmann) contribution to the square of spreading of the quantum state at energy $E$ due to diffusion, averaged on a time scale $\tau$. $L(\tau)$ is bounded by the unit cell length and saturates to a constant value already for short averaging time. The dc conductivity of the system in the crystalline direction $j$ can be written as

$$\sigma_j = \sigma_{Bj} + \sigma_{NBj} = e^2 g(E_F) v_j^2 \tau_j + e^2 g(E_F) \frac{L_j^2(\tau_j)}{\tau_j}, \qquad (1)$$

where $\sigma_{Bj}$ is the Boltzmann contribution and $\sigma_{NBj}$ is the non-Boltzmann contribution. The scattering rate $\tau^{-1}$ will generally be a sum of a temperature- and orientation-independent rate $\tau_0^{-1}$ due to scattering by quenched defects and a temperature-dependent term due to scattering by phonons

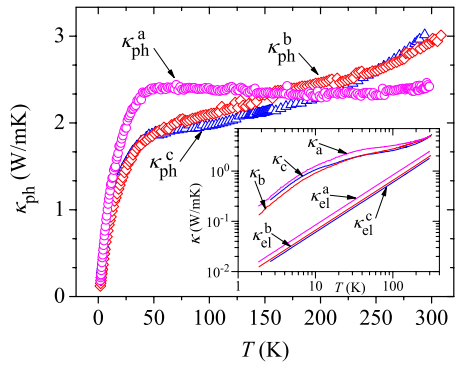


FIG. 6. (Color online) Lattice thermal conductivity $\kappa_{ph}$ of $Al_{80}Cr_{15}Fe_5$ along the three crystalline directions $a$, $b$, and $c$ of the orthorhombic unit cell. The inset shows the total thermal conductivity $\kappa$ and the electronic contribution $\kappa_{el}$ along the three crystalline directions on the logarithmic temperature scale.

$\tau_p^{-1}$. The anisotropy of the atomic structure implies that the phonon spectrum will also be anisotropic, so that the scattering rate will generally depend on the crystalline direction, $\tau_j^{-1}=\tau_0^{-1}+\tau_{pj}^{-1}$. In the simplest case, $\tau_{pj}$ can be phenomenologically written as a power law of temperature, $\tau_{pj}=\beta_j/T^{\alpha_j}$. Assuming that $L_j^2(\tau_j)$ can be replaced by its limiting value, a constant $L_j^2$, Eq. (1) yields a minimum in the conductivity $\sigma_j$ as a function of $\tau_j$ or temperature (or equivalently, there is a maximum in the resistivity $\rho_j=\sigma_j^{-1}$) at the condition $\tau_j=L_j/v_j$. Above the resistivity maximum, the non-Boltzmann contribution prevails and the resistivity will exhibit a nonmetallic NTC, whereas below the maximum, the resistivity will exhibit a metallic PTC due to dominant Boltzmann contribution. The resistivity maxima, as observed for $\rho_b$ and $\rho_c$ in Fig. 1, can thus be considered as a consequence of a crossover from dominant ballistic conductivity at low $T$ to dominant nonballistic conductivity at high $T$ due to small velocities of the charge carriers.

Defining $A_j=e^2g(E_F)v_j^2\tau_0$, $B_j=e^2g(E_F)L_j^2/\tau_0$, and $C_j=\tau_0/\beta_j$, Eq. (1) can be rewritten as

$$\sigma_j = \frac{A_j}{1+C_jT^{\alpha_j}} + B_j(1+C_jT^{\alpha_j}), \qquad (2)$$

which contains four crystalline-direction-dependent fit parameters $A_j$, $B_j$, $C_j$, and $\alpha_j$ (the last two always appear in a product $C_jT^{\alpha_j}$). The zero-temperature conductivity is obtained as $\sigma_j^0=A_j+B_j$. In the regime of dominant scattering by quenched defects, $\tau_0/\tau_{pj}=C_jT^{\alpha_j}\ll 1$, normally realized at low temperatures, expansion of Eq. (2) yields the low-temperature form of the conductivity $\sigma_j=\sigma_j^0-\sigma_1T^{\alpha_j}$ (provided that $A_j>B_j$). This can be viewed as a generalized Bloch-Grüneisen law that yields a metallic PTC resistivity. In the other extreme of dominant phonon scattering, $\tau_0/\tau_{pj}=C_jT^{\alpha_j}\gg 1$, normally realized at high temperatures, Eq. (2) yields the high-temperature form of the conductivity as $\sigma_j=\sigma_2T^{\alpha_j}$, yielding an insulatorlike NTC resistivity. The relative magnitudes of $A_j$, $B_j$, and $C_jT^{\alpha_j}$ coefficients thus determine the temperature dependence of the resistivity within a given temperature range, which can either be in the metallic or insulatinglike regimes, or at a crossover between these two regimes (in which case the resistivity exhibits a maximum). This is shown in Fig. 7, where theoretical resistivities, calculated from Eq. (2), are plotted for different combinations of the coefficients. Since these coefficients depend on the electronic structure of the investigated compound [$g(E_F)$ and $v_j$], its crystallographic details ($L_j$), defect concentration ($\tau_0$), and phononic spectrum ($\tau_{pj}$), they are specific to a given structure and sample purity. It is interesting that for some combination of the $A_j$, $B_j$, $C_j$, and $\alpha_j$ parameters, Eq. (2) gives identical temperature dependence of the resistivity as the theory of weak localization,[23] frequently used to analyze the temperature-dependent resistivity of icosahedral QCs. Weak localization is considered to introduce small temperature-dependent correction $\Delta\sigma_{WL}(T)$ to the Boltzmann conductivity due to spin-orbit and inelastic scattering processes of electrons and is written in the form

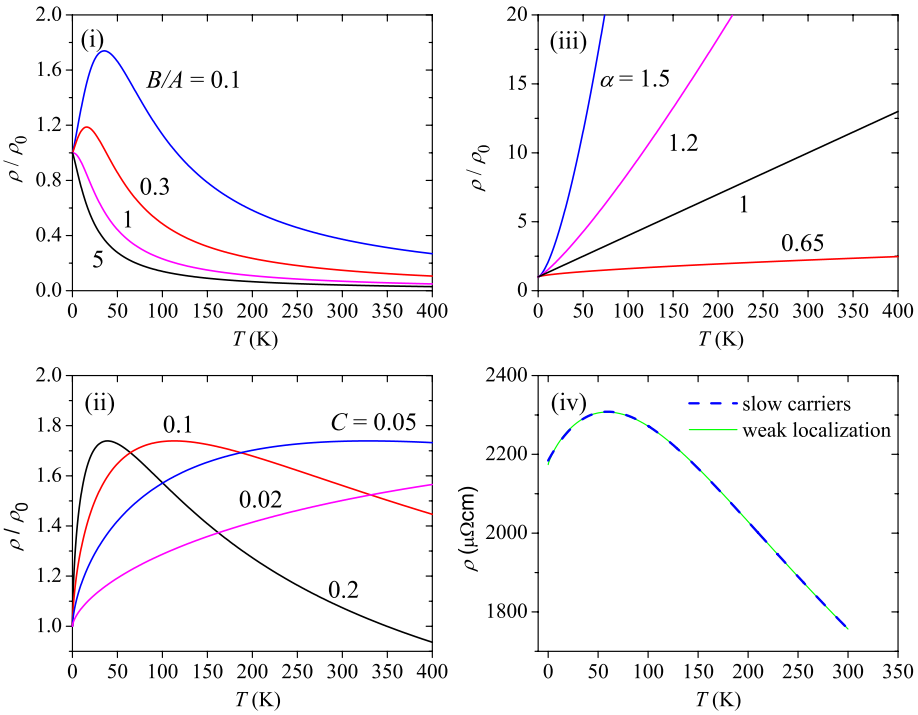


FIG. 7. (Color online) Theoretical temperature-dependent electrical resistivities [normalized to $\rho_0=\rho(T=0)$ value] calculated from Eq. (2) for different combinations of the parameters $B/A$, $C$, and $\alpha$ (the subscript $j$, denoting the crystalline direction, has been omitted). In panel (i), the ratio $B/A$ is varied while keeping fixed $C=0.03$ and $\alpha=1.2$. In panel (ii), $B/A=0.1$ and $\alpha=0.65$ are fixed and $C$ is varied. Very similar temperature-dependent resistivities are also obtained by keeping $B/A$ and $C$ constant and varying $\alpha$. This is due to the fact that $C$ and $\alpha$ appear in a product $CT^{\alpha}$ in Eq. (2). Panel (iii) shows the case where $B/A=1\times10^{-7}$ (corresponding to the extreme Boltzmann regime) and $C=0.03$ are kept constant and $\alpha$ is varied. Similar temperature dependencies are obtained by keeping $B/A$ and $\alpha$ constant and varying $C$. Panel (iv) shows comparison of the temperature-dependent resistivities for two models: the model of slow charge carriers of Eq. (2) using the set of parameters $A=3.03\times10^{-4}$ $\mu\Omega$ cm, $B/A=0.51$, $C=0.065$, and $\alpha=1.0064$ and the model of weak localization, $\sigma=\sigma_0+\Delta\sigma_{WL}$, with $\Delta\sigma_{WL}$ given by Eq. (3). For the weak localization curve, we applied the set of parameters used previously (Ref. 24) to reproduce the temperature-dependent resistivity of icosahedral $Al_{70.5}Pd_{21.2}Mn_{8.3}$ QC: $\sigma_0=4.6\times10^{-4}$ $(\mu\Omega\ \text{cm})^{-1}$, $e^2/(2\pi^2\hbar\sqrt{D\tau_{so}})=1.55\times10^{-4}$ $(\mu\Omega\ \text{cm})^{-1}$, and, by rewriting $t=(T/T_0)^{\alpha}$, $T_0=207$ K and $\alpha=1.66$. The two curves are indistinguishable.

$$\Delta\sigma_{WL}(T)=\frac{e^2}{2\pi^2\hbar\sqrt{D\tau_{so}}}(3\sqrt{t+1}-\sqrt{t}-3), \tag{3}$$

where $D$ is the diffusion constant, $\tau_{so}$ the spin-orbit scattering time, and $t=\tau_{so}/4\tau_i(T)$, where $\tau_i(T)$ is the inelastic scattering time. Considering $\tau_i\propto 1/T^{\alpha}$ [the same form as used in Eq. (2)], sets of parameters pertinent to Eqs. (2) and (3) can be found that yield identical temperature dependence of the resistivity, exhibiting a maximum in the low-temperature regime. Such comparison is shown in Fig. 7, panel (iv), where it is evident that Eqs. (2) and (3) give indistinguishable curves [quantitative details of this comparison are given in the caption to Fig. 7(iv)]. However, while the validity of the weak localization concept is restricted to low temperatures, the theory of slow charge carriers of Eq. (2) is applicable at all temperatures and does not involve any electron localization.

The fits of the resistivities with Eq. (2) are displayed in Fig. 1 as solid lines and the fit parameters are collected in Table III. The fits are excellent for all three crystalline directions. The $A_j$ parameter values enable us to estimate the anisotropy of the electronic average velocities along the three

TABLE III. Fit parameters of the electrical resistivity [solid curves in Fig. 1, as calculated from Eq. (2)]. The units of the coefficients $C_j$ are chosen so that the temperature in the expression $C_jT^{\alpha_j}$ is dimensionless.

| | | | |
|---|---|---|---|
| Crystalline direction $a$ | | | |
| $A_a$ $(\mu\Omega\ \text{cm})^{-1}$ | $B_a$ $(\mu\Omega\ \text{cm})^{-1}$ | $C_a$ | $\alpha_a$ |
| $2.16\times10^{-3}$ | $1.32\times10^{-3}$ | $4.40\times10^{-3}$ | 0.70 |
| Crystalline direction $b$ | | | |
| $A_b$ $(\mu\Omega\ \text{cm})^{-1}$ | $B_b$ $(\mu\Omega\ \text{cm})^{-1}$ | $C_b$ | $\alpha_b$ |
| $1.70\times10^{-3}$ | $1.04\times10^{-3}$ | $1.27\times10^{-2}$ | 0.64 |
| Crystalline direction $c$ | | | |
| $A_c$ $(\mu\Omega\ \text{cm})^{-1}$ | $B_c$ $(\mu\Omega\ \text{cm})^{-1}$ | $C_c$ | $\alpha_c$ |
| $1.57\times10^{-3}$ | $9.34\times10^{-4}$ | $2.06\times10^{-2}$ | 0.57 |

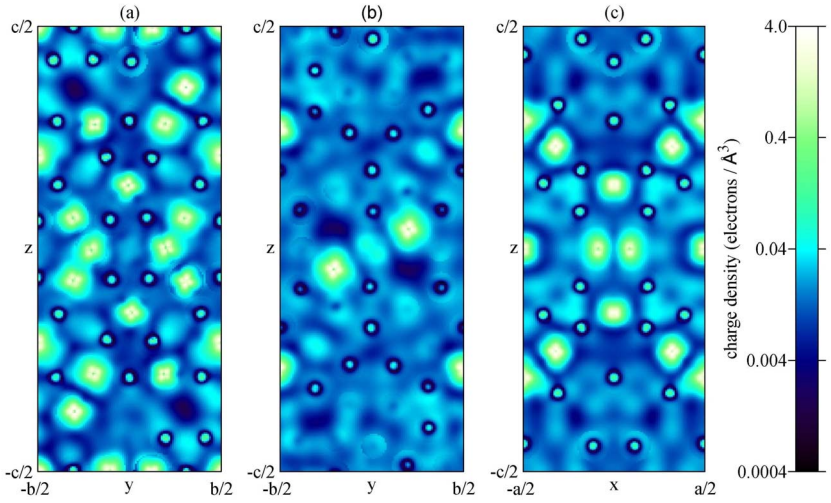


FIG. 8. (Color online) Electronic charge density of the relaxed model of $Al_4(Cr,Fe)$ calculated in the energy interval $(E_F-0.5\ \text{eV}, E_F+0.5\ \text{eV})$. The panels show (a) the $x=0$ (flat layer $F$), (b) the $x \approx a/6$ (puckered layer $P$), and (c) the $y=0$ planes.

crystalline directions. We get $v_a/v_b=\sqrt{A_a/A_b}=1.13$, $v_a/v_c=1.17$, and $v_b/v_c=1.04$, so that the velocity is the highest along the $a$ axis perpendicular to the atomic planes and there is also a small anisotropy within the atomic planes. The parameters $C_j$ and $\alpha_j$ describe the anisotropy of the electron-phonon scattering rate. Anisotropy of the phononic spectrum is reflected in the anisotropy of the lattice thermal conductivity $\kappa_{ph}$ shown in Fig. 6. The observed anisotropy of $\kappa_{ph}$ thus gives qualitative support to the presumption that the phononic spectrum of $Al_{80}Cr_{15}Fe_5$ is spatially anisotropic and justifies the use of a crystalline-direction-dependent phonon scattering rate $\tau_{pj}^{-1}$.

The very different temperature-dependent electrical resistivities of $Al_{80}Cr_{15}Fe_5$ along the three crystalline directions can thus be all treated within the same physical model of slow charge carriers, where the increased electron-phonon scattering upon raising the temperature induces a transition from dominant Boltzmann (metallic) to dominant non-Boltzmann (insulatinglike) regime. As this happens in the presence of a high density of charge carriers, the temperature dependence of the resistivity is governed predominantly by the temperature dependence of the electronic diffusion constant $D$ and the transition has no resemblance to the Anderson-type metal-to-insulator transition based on gradual electron localization. The metalliclike $\rho_a(T)$ in Fig. 1 is nothing but the low-$T$ part of the $\rho_b(T)$- and $\rho_c(T)$-type resistivities. The above considerations also reveal that the broad maximum in $\rho(T)$ is not a magnetic effect, as considered previously in the context of $i$-Al-Pd-Mn QCs with the same type of temperature-dependent resistivity.[24]

## V. TRANSPORT ANISOTROPY VERSUS COMPLEX ATOMIC ORDER

The above model considers the anisotropy of the electrical resistivity (as well as of the other electrical and thermal transport coefficients) of the $Al_{80}Cr_{15}Fe_5$ decagonal approximant to arise from the anisotropy of its electronic structure and phonon spectrum. These quantities depend crucially on the anisotropy of the atomic structure, i.e., on the microscopic structural details of the $Al_4TM$ phase along different crystallographic directions. We, therefore, consider possible reasons for the anisotropy of the resistivity by analyzing structural details of our relaxed version of the model of Deng *et al.* To this end, we first calculated *ab initio* the electronic charge density within the $Al_4TM$ unit cell in a narrow window around the Fermi energy ($E_F-0.5$ eV, $E_F+0.5$ eV), corresponding roughly to the electron density that actually participates in the conduction process. This window is indicated as a gray hatched area in Fig. 5 of the DOS. The charge density maps are shown in Fig. 8 for the same planes ($F$, $P$, and $y=0$), for which the atomic positions of the relaxed model are also displayed in Fig. 4. It is observed that the Cr and Fe atoms light up brightly, indicating a strongly peaked charge density on the TM atoms, whereas the Al atoms are darker (smaller charge density), but the density between them is more uniform and hence electron-gas-like. Two more details can be noticed in Fig. 8: the four-lobe structure of the high charge density on most of the TM atoms, which is typical for the $d$ orbitals, and the discontinuities (small black circles) that can be seen in the charge density at the boundaries of the atomic spheres. The latter effect is an artifact of the LAPW method and has no physical significance. In the electronic long-range transport, the conduction electrons will preferentially move along connected paths of uniform charge density from one to another end of the sample. High conductivity in a given crystallographic direction can then be expected in case that atomic chains of predominantly Al atoms in direct contacts propagate along this direction. In the following, we will make an analysis of the atomic chain distribution along the $a$, $b$, and $c$ crystallographic directions of the $Al_4TM$ structure.

We describe the analysis for the $a$ direction, whereas those for the $b$ and $c$ directions are analogous. Using the model of Deng *et al.*, we constructed a "supercell" of two unit cells stacked along $a$ and took one of the atoms located within the "left" $(b,c)$ boundary plane of the supercell (denoted as "atom 1") to be the origin of a chain. The vectors joining atom 1 to its $j$ nearest neighbors are denoted as $\vec{r}_{1j}$. The angles $\theta_{1j}$ between $\vec{r}_{1j}$ and the $a$ direction [described by the unit vector $\hat{a}=(1,0,0)$] were then determined by the sca-

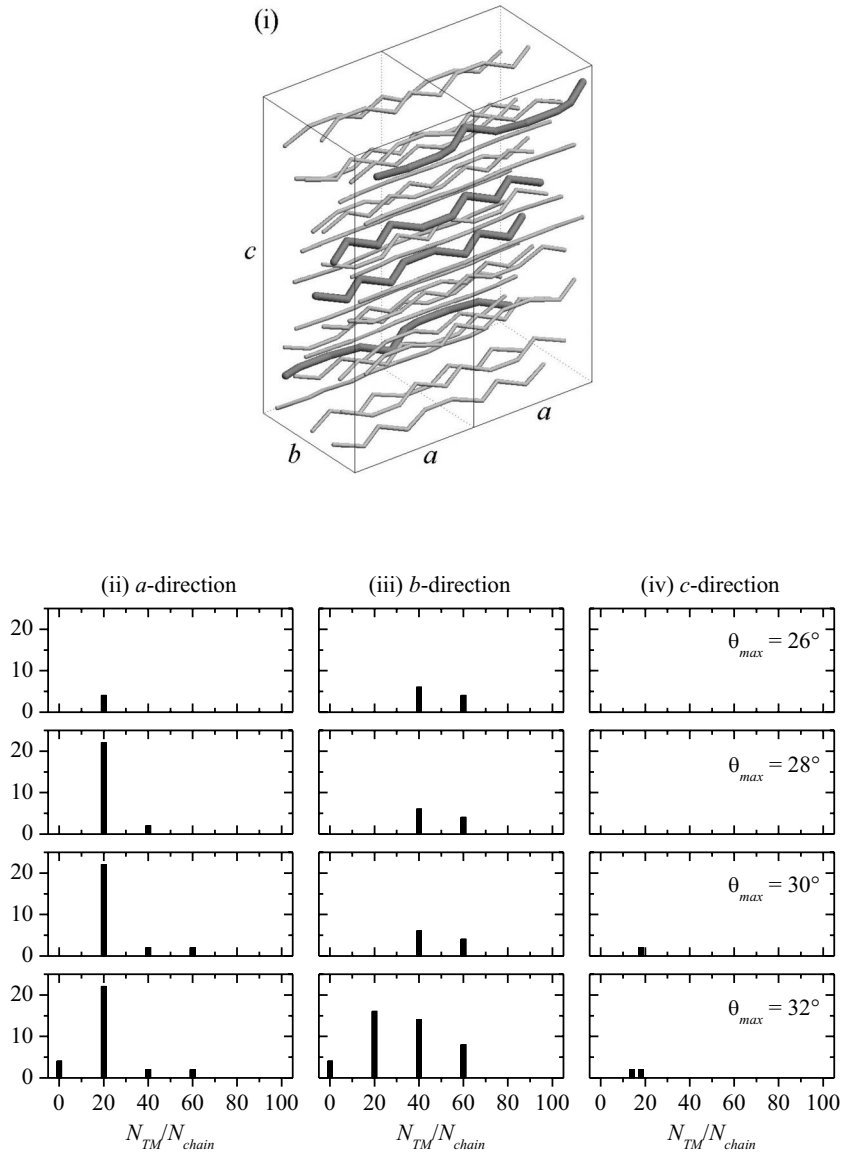


FIG. 9. (i) Visualization of the atomic chains for $\theta_{\max}=32°$ along the $a$ direction of the $Al_4TM$ supercell composed of two unit cells. Pure Al chains are drawn by thicker lines. Histograms, showing the number of chains in the supercell and their distribution according to the $N_{TM}/N_{chain}$ criterion for various $\theta_{\max}$, are displayed in other three panels [panel (ii), $a$ direction; panel (iii), $b$ direction; panel (iv), $c$ direction]. $N_{TM}/N_{chain}$ is given in %.

lar product $\vec{r}_{1j}\cdot\hat{a}=r_{1j}\cos\theta_{1j}$. Those nearest neighbors were selected that were lying closest to the $a$ direction by satisfying a criterion $\theta_{1j}<\theta_{\max}$, where $\theta_{\max}$ is a preselected maximum allowed angle. Each of these atoms was then taken as "atom 2" of a particular atomic chain. The same step was then repeated until the chains (of a common ancestor atom 1) reached the "right" $(b,c)$ boundary plane of the supercell. The procedure was then repeated for all atoms lying within the left boundary plane. In this way, constructed atomic sequences form zigzag chains with all $\theta_{ij}<\theta_{\max}$ [Fig. 9, panel (i)] and represent the shortest connections along the $a$ direction over the supercell. Large majority of the so-constructed chains contained 10 atoms, whereas some with 11 atoms were also found. The nearest-neighbor distances were distributed within the range 2.3–3.1 Å with the peak at 2.7 Å, thus excluding the possibility that some next-nearest-neighbor atoms could also participate in the chains. In many cases, different chains contained a considerable fraction of common atoms, making them very similar. Only the chains that contained less than 50% of common atoms were considered to be different.

In counting the chains, we used two criteria. We first specified $\theta_{\max}$ and observed how many chains are present in the structure along $a$ (the smaller the $\theta_{\max}$, the more straight is the chain). $\theta_{\max}$ was varied between 26° and 32°. The second criterion was the percentage of TM atoms in the chain, given by the ratio $N_{TM}/N_{chain}$. As there were typically ten atoms in one chain over the supercell (thus five atoms in one unit cell), the ratio, e.g., $N_{TM}/N_{chain}=0.2$, means that one out of five atoms in one unit cell is TM and the remaining

four are Al. The chains with small number of TM atoms are then considered to be more conducting (following the *ab initio* result that the charge density between nearest-neighbor Al atoms is more uniform and electron-gas-like).

Histograms, showing the number of chains and their distribution according to the $N_{TM}/N_{chain}$ criterion for various $\theta_{\max}$ along the three crystalline directions, are displayed in Fig. 9. For the smallest $\theta_{\max}=26°$, the *a* direction [panel (ii)] already contains chains with a small number of TM atoms ($N_{TM}/N_{chain}=0.2$), whereas the chains along *b* [panel (iii)] contain more TM atoms ($N_{TM}/N_{chain}=0.4$ and 0.6). For the *c* direction [panel (iv)], no connected chains can be found for this choice of $\theta_{\max}$. Increasing $\theta_{\max}$ toward 32°, the chains $N_{TM}/N_{chain}=0.2$ are present along *a* for all choices of $\theta_{\max}$ (with their number saturated at 22), whereas for the *b* direction, such chains appear only at the largest $\theta_{\max}=32°$ (being 16 in number). For this choice of $\theta_{\max}$, some pure Al chains ($N_{TM}/N_{chain}=0$) also exist for the *a* and *b* directions [shown by thicker lines in Fig. 9(i)]. For the *c* direction, connected chains (small in number) appear only at $\theta_{\max}$ higher than 30°. The Al-rich chains along the *a* direction perpendicular to the atomic planes are thus more straight (shorter) than those within the $(b,c)$ atomic planes and the number of chains with small $\theta_{\max}$ is the highest for the *a* direction, making it the most conducting direction. The same consideration suggests that the *c* direction is the least conducting one. The above chain-distribution analysis, based on the specific structural details of the complex atomic order of the $Al_4TM$ phase along the three crystallographic directions, thus qualitatively accounts for the anisotropy of the electrical resistivity of $Al_{80}Cr_{15}Fe_5$. This anisotropy is a consequence of the specific complex local atomic order within the giant unit cell of the $Al_4TM$ phase on the scale of nearest-neighbor atoms and has little (or nothing) to do with symmetries of the intermediate-scale structural motifs and atomic clusters within the unit cell, where the icosahedral nearest-neighbor coordination prevails.

## VI. DISCUSSION AND CONCLUSIONS

The choice of the $Al_{80}Cr_{15}Fe_5$ complex metallic alloy to study the anisotropic transport properties in relation to *d*-QCs appears to be advantageous. This compound is an excellent periodic approximant to the decagonal phase and single-crystalline samples of high structural perfection could recently be grown. Due to the six-layer structure of the $Al_4TM$ phase, the anisotropy in the transport properties is smaller than that in the two- and four-layer structures, but still pronounced. The important point is that the velocity of the charge carriers is just in the range where temperature induces transition from dominant Boltzmann (metallic) to dominant non-Boltzmann (insulatinglike) regimes, as demonstrated in the appearance of the resistivity maximum for specific crystalline directions. Consequently, a temperature-dependent electronic diffusion coefficient pertinent to slow charge carriers enables the unified treatment of both regimes. This situation is less evident in the more anisotropic two- and four-layer *d*-QCs, where the very different magnitudes and temperature dependencies of $\rho_P$ and $\rho_Q$ seem to be uncorrelated at the first glance. However, assuming that the velocities along the *P* and *Q* directions are in this case in the extreme Boltzmann and non-Boltzmann regimes, respectively, enables treatment of the more anisotropic *d*-QCs on the same footing of slow charge carriers. A single physical picture thus applies to Al-TM-type *d*-QCs at all temperatures and for all crystalline directions, either periodic or quasiperiodic. The anisotropy of the resistivity is ultimately related to the anisotropy of the electronic band structure that is responsible for the anisotropy of the electronic velocity along different crystalline directions. A preliminary discussion of the velocity anisotropy in *d*-QCs in relation to the number of quasiperiodic layers within one periodic unit is given elsewhere,[11] where the two-layer case is shown to be the most anisotropic one.

The above approach of slow charge carriers has been successfully applied to the electrical resistivity, whereas implementation of this concept to other transport coefficients still has to be performed. At present, we cannot offer quantitative explanation of the anisotropic thermopower shown in Fig. 2 that shows complicated temperature dependence with minima and maxima. Phonon drag effect, which sometimes yields a minimum in $S(T)$, may be present as well. Hall coefficient (Fig. 3) shows a pronounced anisotropy. For the current flow along the *a* direction perpendicular to the $(b,c)$ atomic layers, different signs of $R_H$ are obtained for the magnetic field directed along either of the two in-plane directions *b* and *c*. This indicates a complicated shape of the Fermi surface and suggests coexistence of pockets of electrons and holes. A determination of the Fermi surface for the $Al_4TM$ structure is needed in order to explain the anisotropy of the Hall coefficient. Similar consideration also applies to the phonon thermal conductivity shown in Fig. 6, where the analysis of the $\kappa_{ph}$ anisotropy requires knowledge of the vibrational DOS specific to the $Al_4TM$ structure.

Recalling the three fundamental questions raised in the Introduction, we are able to give the following answers.

(i) The origin of nonmetallic transport in the presence of a high density of charge carriers is their slow velocity. The NTC of the resistivity is a consequence of a specific temperature dependence of the electronic diffusion coefficient due to non-Boltzmann (nonballistic) motion of charge carriers.

(ii) The model of slow charge carriers gives a unified picture of the electronic transport along the *Q* and *P* directions in *d*-QCs and their approximants. Temperature effects (increased electron-phonon scattering) can induce transition from dominant metallic to dominant insulatinglike regime. The transition occurs in the presence of a high density of charge carriers and has no resemblance to the Anderson-type metal-to-insulator transition due to gradual electron localization. The very different magnitudes and temperature dependencies of $\rho_Q$ and $\rho_P$ observed in the most anisotropic *d*-QCs with two atomic layers in one periodicity unit can be explained within the same physical model, considering anisotropic band structure and the associated differences in the electronic velocities.

(iii) The anisotropy of the transport properties is a consequence of the complex local atomic order on the scale of nearest-neighbor atoms and has little (or nothing) to do with

symmetries of the intermediate-scale structural motifs and atomic clusters, either periodic or quasiperiodic. This suggests that the role of quasiperiodicity in the anisotropic transport of *d*-QCs is marginal, if not negligible.

Finally, the concept of slow charge carriers does not seem to be restricted to *d*-QCs and their approximants only. Very similar temperature-dependent resistivities, exhibiting a broad maximum of practically identical shape to that displayed in Figs. 1(a) and 1(b), though with much higher absolute values (of up to several 1000 $\mu\Omega$ cm) were observed also in icosahedral QCs, the most studied example being *i*-Al-Pd-Mn.[25–28] The much higher $\rho$ values can be attributed to the reduced DOS at $E_F$ due to the pseudogap in icosahedral QCs.

## ACKNOWLEDGMENTS

This work was done within the activities of the 6th Framework EU Network of Excellence "Complex Metallic Alloys" (Contract No. NMP3-CT-2005-500140). A.S. acknowledges support by the Ministry of Science, Education and Sports of the Republic of Croatia through the Research Project No. 177-0352828-0478 "Transport and magnetic properties of nanostructured complex metallic compounds."

*Permanent address: Faculty of Natural Sciences, Mathematics and Education, University of Split, Croatia.

[1] T. Shibuya, T. Hashimoto, and S. Takeuchi, J. Phys. Soc. Jpn. **59**, 1917 (1990).
[2] S. Martin, A. F. Hebard, A. R. Kortan, and F. A. Thiel, Phys. Rev. Lett. **67**, 719 (1991).
[3] Wang Yun-ping and Zhang Dian-lin, Phys. Rev. B **49**, 13204 (1994).
[4] Lin Shu-yuan, Wang Xue-mei, Lu Li, Zhang Dian-lin, L. X. He, and K. X. Kuo, Phys. Rev. B **41**, 9625 (1990).
[5] Zhang Dian-lin, Lu Li, Wang Xue-mei, Lin Shu-yuan, L. X. He, and K. H. Kuo, Phys. Rev. B **41**, 8557 (1990).
[6] Wang Yun-ping, Zhang Dian-lin, and L. F. Chen, Phys. Rev. B **48**, 10542 (1993).
[7] Zhang Dian-lin, Cao Shao-chun, Wang Yun-ping, Lu Li, Wang Xue-mei, X. L. Ma, and K. H. Kuo, Phys. Rev. Lett. **66**, 2778 (1991).
[8] K. Edagawa, M. A. Chernikov, A. D. Bianchi, E. Felder, U. Gubler, and H. R. Ott, Phys. Rev. Lett. **77**, 1071 (1996).
[9] D. N. Basov, T. Timusk, F. Barakat, J. Greedan, and B. Grushko, Phys. Rev. Lett. **72**, 1937 (1994).
[10] M. Krajčí and J. Hafner, Phys. Rev. B **58**, 5378 (1998).
[11] G. Trambly de Laissardière and T. Fujiwara, Phys. Rev. B **50**, 9843 (1994).
[12] Z. M. Stadnik, G. W. Zhang, A.-P. Tsai, and A. Inoue, Phys. Rev. B **51**, 11 358 (1995).
[13] R. F. Sabiryanov, S. K. Bose, and S. E. Burkov, J. Phys.: Condens. Matter **7**, 5437 (1995).
[14] M. Krajčí, J. Hafner, and M. Mihalkovič, Mater. Sci. Eng., A **294-296**, 548 (2000).
[15] P. Volkov and S. J. Poon, Phys. Rev. B **52**, 12685 (1995).
[16] D. W. Deng, Z. M. Mo, and K. H. Kuo, J. Phys.: Condens. Matter **16**, 2283 (2004).
[17] P. Blaha, K. Schwarz, G. K. H. Madsen, D. Kvasnicka, and J. Luitz, *WIEN2K, An Augmented Plane Wave + Local Orbitals Program for Calculating Crystal Properties* (Techn. Universitaet Wien, Vienna, Austria, 2001).
[18] J. P. Perdew and Y. Wang, Phys. Rev. B **45**, 13244 (1992).
[19] D. Singh, Phys. Rev. B **43**, 6388 (1991).
[20] E. Sjöstedt, L. Nordström, and D. J. Singh, Solid State Commun. **114**, 15 (2000).
[21] G. K. H. Madsen, P. Blaha, K. Schwarz, E. Sjöstedt, and L. Nordström, Phys. Rev. B **64**, 195134 (2001).
[22] G. Trambly de Laissardière, J.-P. Julien, and D. Mayou, Phys. Rev. Lett. **97**, 026601 (2006).
[23] H. Fukuyama and K. Hoshino, J. Phys. Soc. Jpn. **50**, 2131 (1981).
[24] J. Dolinšek, M. Klanjšek, Z. Jagličić, A. Bilušić, and A. Smontara, J. Phys.: Condens. Matter **14**, 6975 (2002).
[25] P. Lanco, T. Klein, C. Berger, F. Cyrot-Lackmann, G. Fourcaudot, and A. Sulpice, Europhys. Lett. **18**, 227 (1992).
[26] H. Akiyama, T. Hashimoto, T. Shibuya, K. Edagawa, and S. Takeuchi, J. Phys. Soc. Jpn. **62**, 939 (1993).
[27] M. Rodmar, B. Grushko, N. Tamura, K. Urban, and Ö. Rapp, Phys. Rev. B **60**, 7208 (1999).
[28] R. Escudero, J. Lasjaunias, Y. Calvayrac, and M. Boudard, J. Phys.: Condens. Matter **11**, 383 (1999).